Bias- and Geometry-Dependent Ionization Effects on Waveguide-Integrated Germanium-on-Silicon p-i-n Photodiodes

Anurag R. Veluri, *Graduate Student Member, IEEE*, Kellen P. Arnold, *Member, IEEE*, Solomon Musibau, *Member, IEEE*, Artemisia Tsiara, Kristof Croes, Dimitri Linten, Joris Van Campenhout, *Member, IEEE*, Steven L. Kosier, *Senior Member, IEEE*, Ronald D. Schrimpf, *Life Fellow, IEEE*, Daniel M. Fleetwood, *Life Fellow, IEEE*, Robert A. Reed, *Fellow, IEEE*, and Sharon M. Weiss, *Senior Member, IEEE*

***Abstract*—This work investigates the waveguide-integrated vertical p-i-n (VPIN) germanium-on-silicon (Ge-Si) photodiodes under 10-keV X-ray irradiation to evaluate the impact of geometrical features, implant design, and bias during irradiation on total ionizing dose (TID) response. The use of localized p^+ contact implantation for high efficiency leads to heightened TID sensitivity, due to ionization-induced oxide trapped charges at the top Ge/SiO_2 interface. This more than doubles the dark current, as compared to designs with continuous contact doping. The TID-induced response of each photodiode design is strongly influenced by bias during irradiation, with increases in dark current up to ~100% for −2 V bias, compared to grounded test conditions. This increase is due to electric field enhancement near the Ge/SiO_2 interface, as demonstrated by technology computer-aided design (TCAD) simulations. The application of forward bias after irradiation leads to swift annealing of TID effects and partial performance recovery due to injection-enhanced tunneling near the Ge/SiO_2 interface. The observed dark current sensitivities and mitigation by forward bias annealing suggest that Ge-Si photodiodes are well-suited for applications in high-radiation environments.**

***Index Terms*—Annealing, bias dependence, germanium-on-silicon (Ge-Si) photodiodes, photonic integrated circuits (PICs), radiation effects, silicon photonics, total ionizing dose (TID).**

Received 8 October 2025; revised 10 November 2025; accepted 12 November 2025. Date of publication 14 November 2025; date of current version 24 April 2026. The work of Kellen P. Arnold was supported by the National Aeronautics and Space Administration (NASA) Space Technology Graduate Research Opportunities (NSTGRO) 2023 under Grant 80NSSC23K1198. This work was supported in part by the Fonds Wetenschappelijk Onderzoek under Grant V439524N, in part by the National Science Foundation (NSF) Industry-University Cooperative Research Center (IUCRC) Electronic-Photonic Integrated Circuits for Aerospace (EPICA) under Grant 2052742, in part by the NSF EPICA Industry Advisory Board (IAB), and in part by the Air Force Office of Scientific Research (AFOSR) Defense University Research Instrumentation Program (DURIP) Award under Grant FA9550-22-1-0471. *(Corresponding author: Anurag R. Veluri.)*

Anurag R. Veluri and Steven L. Kosier are with the Department of Electrical and Computer Engineering, Vanderbilt University, Nashville, TN 37235 USA (e-mail: anurag.reddy.veluri@vanderbilt.edu; steven.kosier@vanderbilt.edu).

Kellen P. Arnold is with the Interdisciplinary Materials Science Program, Vanderbilt University, Nashville, TN 37235 USA (e-mail: kellen.p.arnold@vanderbilt.edu).

Solomon Musibau is with imec, 3001 Leuven, Belgium, and also with the Katholieke Universiteit Leuven, 3001 Leuven, Belgium (e-mail: solomon.musibau@imec.be).

Artemisia Tsiara, Kristof Croes, Dimitri Linten, and Joris Van Campenhout are with imec, 3001 Leuven, Belgium (e-mail: artemisia.tsiara@imec.be; kristof.croes@imec.be; dimitri.linten@imec.be; joris.vancampenhout@imec.be).

Ronald D. Schrimpf, Daniel M. Fleetwood, Robert A. Reed, and Sharon M. Weiss are with the Department of Electrical and Computer Engineering and the Interdisciplinary Materials Science Program, Vanderbilt University, Nashville, TN 37235 USA (e-mail: ron.schrimpf@vanderbilt.edu; dan.fleetwood@vanderbilt.edu; robert.reed@vanderbilt.edu; sharon.weiss@vanderbilt.edu).

Color versions of one or more figures in this article are available at https://doi.org/10.1109/TNS.2025.3633166.

Digital Object Identifier 10.1109/TNS.2025.3633166

I. Introduction

The emergence of silicon photonics for the next-generation optical data transmission links promises significant advantages in terms of size, weight, and power consumption over discrete optical and electrical communications systems [1]. The inherent compatibility of silicon photonics with well-established complementary metal–oxide–semiconductor (CMOS) fabrication processes enables high-volume, cost-effective manufacturing and facilitates monolithic integration of photonic and electronic integrated circuits in a unified platform [2], [3], [4]. For fully integrated systems, the on-chip, waveguide-coupled photodiodes play a pivotal role, enabling data conversion from the optical to electrical domains for downstream processing. At near-infrared wavelengths, which are widely used in data communications, germanium (Ge) is a particularly attractive solution due to its exceptional absorption properties and fast optoelectronic response. In photonic integrated circuits (PICs), germanium-on-silicon (Ge-Si) waveguide-integrated p-i-n photodiodes have become widely adopted. These devices offer high responsivity, fast operation, and are compatible with silicon photonics platforms, making them ideal for electronic readout from PICs [5], [6].

Over the last decade, interest in silicon photonics has grown for a wide variety of space mission applications, including atmospheric sensing, satellite communications, navigation, and LiDAR [7], [8], [9]. However, for PIC components to be viable in space, their performance in harsh radiation environments must be thoroughly evaluated [10], [11]. Recent progress has been made in understanding radiation-induced damage mechanisms and reliability considerations for silicon photonic devices, including waveguides [12],

[13], [14], [15], modulators [16], [17], [18], [19], [20], and ring resonators [21], [22]. For on-chip integrated photodiodes, sensitivity to single-event transients (SETs) has been shown, with both applied bias voltage and specific design choices playing an important role [23], [24]. Cumulative damage effects due to total ionizing dose (TID) and displacement damage have also been investigated [17], [25], [26], [27], [28]. Studies on ionization effects in Ge-Si photodiodes have shown minimal impact on responsivity and high-speed performance, isolating radiation sensitivity at dose levels relevant to space to increased dark current, which constitutes the noise floor in PIC operation. While the reported dark current increases are moderate, these increases may become significant as the performance requirements and complexity of PICs increase. However, understanding of the influence of bias during irradiation, geometrical and implant design parameters, and post-irradiation annealing effects is lacking. A comprehensive understanding of these factors is important to inform future design choices and recovery strategies for complex PICs in harsh radiation environments.

In this work, we evaluate the impact of geometrical features, implant design, and bias during 10-keV X-ray irradiation on the TID response of Ge-Si vertical p-i-n (VPIN) photodiodes that have been designed to meet different speed and efficiency performance requirements. We find that utilizing a localized p^+ contact implant leads to greater TID susceptibility at standard operating voltage, resulting in a relative dark current increase that is more than twice as large as that of designs with continuous contact implants under grounded irradiation. The higher TID susceptibility is attributed to ionization-induced oxide trapped charge at the p^+Ge/i-Ge junction near the top Ge/SiO_2 interface. Moreover, TID effects on each photodiode design are strongly influenced by the bias applied during irradiation, with increases in dark current up to ~100% for −2 V operating condition compared to the grounded irradiation. This enhanced sensitivity is attributed to the increased electric field near the Ge/SiO_2 interface, which increases the noise floor level of the system. However, the application of forward bias after irradiation leads to rapid annealing of the TID-induced degradation by more than 50% due to injection-enhanced tunneling near the Ge/SiO_2 interface. This work demonstrates the importance of understanding TID effects at operating bias conditions, while also using grounded irradiation to understand the design tradeoffs of device performance and radiation tolerance at typical operating voltages in photonic component design.

II. Device Structure and Experimental Setup

The Ge-Si VPIN photodiodes investigated in this study were fabricated in imec's iSiPP50G 200-mm SOI platform [29]. The three devices are labeled according to the specific performance requirements for which they were designed: VPIN-UHS (ultrahigh speed), VPIN-HS (high speed), and VPIN-HE (high efficiency) [30]. All devices have a silicon (Si) waveguide thickness of 220 nm and Ge thickness of 400 nm. Each device differs in Ge length, Ge width, and Ge p^+ doping geometry, as described in Table I and illustrated in the cross-sectional schematics shown in Fig. 1. VPIN-UHS has a compact Ge width (x-direction) of 1 μm for a reduced RC constant to achieve a larger electrooptic 3-dB bandwidth. VPIN-HS has a Ge width of 2 μm to improve the overlap of the optical mode with the active region of the photodiode, providing a balance between high responsivity and high-speed performance. VPIN-UHS and VPIN-HS have continuous p^+ contact doping along the device length, while VPIN-HE has localized p^+ doping under the metal contact plugs in the Ge layer along the device length and width. Combined with localized p^+ implantation, VPIN-HE also features a longer contact pitch (z-direction), which reduces metal absorption and enhances device responsivity [31].

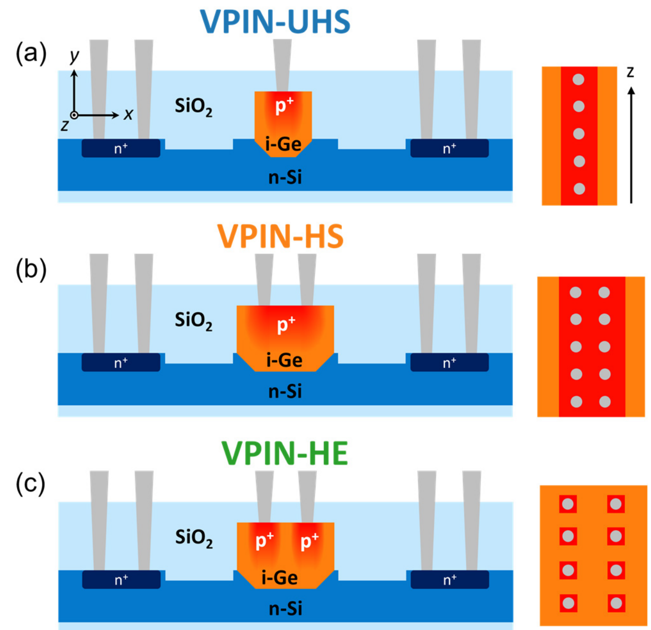

Fig. 1. Cross-sectional schematic view of the three Ge-Si VPIN photodiodes. (a) VPIN-UHS, (b) VPIN-HS, and (c) VPIN-HE. The Ge length and width are along the z- and x-axes, respectively. The contact doping implant design is shown on the right for each structure in the length (z-axis) and width (x-axis), continuous p^+ doping for VPIN-UHS and VPIN-HS and localized p^+ doping for VPIN-HE structure.

TABLE I
Physical Parameters of Ge-Si Photodiodes

Device	VPIN-UHS	VPIN-HS	VPIN-HE
Ge length (μm)	15.2	15.4	13.7
Ge width (μm)	1	2	2
Contact Pitch (μm)	0.6	0.6	0.9
Ge p^+ contact doping	Continuous	Continuous	Localized

Tested chips were mounted using quick-dry silver paste onto a custom-made printed circuit board (PCB) equipped with solder-mounted sub-miniature version A (SMA) terminals for electrical connections. The bond pads connecting the anode and cathode of each PD were ball-bonded to the PCB using 0.7 mil (~18 μm) gold wire, with all anodes sharing a common terminal. Test chips were selected based on their low pre-irradiation dark current, consistent with imec process yield specifications. A Keithley 2400 source-meter and Keysight B1500 parameter analyzer were used to measure the I–V and

TABLE II
DESCRIPTION OF EXPERIMENTAL CONDITIONS AND IRRADIATED SAMPLES

Experiment	Bias during irradiation	*I-V* sweep measurement	Number of devices tested (VPIN-UHS,VPIN-HS, VPIN-HE)
10-keV X-rays	Grounded	-2 to 0 V	(3,3,3)
10-keV X-rays	-2 V	-2 to 0 V	(6,6,5)

time dependent current characteristics at specific bias voltages. Keithley 2230 multi-channel power meters were used to bias devices during irradiation experiments.

X-ray irradiations were performed at Vanderbilt University using an ARACOR 10-keV X-ray irradiator at a dose rate of 28.14 krad(SiO_2)/min. The devices were irradiated in a step-stress method up to 2 Mrad(SiO_2). During biased (−2 V) irradiation, the applied voltage was switched off immediately after each irradiation step, before the device was measured. Dark current *I*–*V* measurements were performed in situ, starting 3 min after each radiation exposure was completed. Each *I*–*V* sweep was performed from −2 to 0 V to avoid injection-enhanced annealing effects, which are discussed in detail in Section III-C. Table II summarizes the experimental conditions and the number of samples of each device structure used for irradiation experiments.

Electric potential and field profiles of all three photodiode structures at 0 and −2 V were extracted from process-calibrated technology computer-aided design (TCAD) simulations using the Synopsys Sentaurus tool to understand the bias dependence on degradation mechanisms under TID irradiation. The TCAD simulation methodology used in this study is described in [32] and [34].

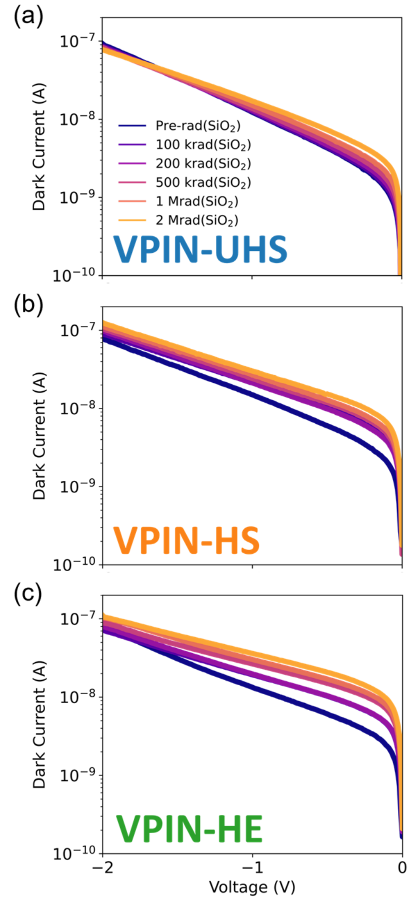

Fig. 2. Representative 10-keV X-ray irradiation results. All devices were grounded during exposure. Dark current *I*–*V* characteristics during X-ray irradiation of (a) VPIN-UHS, (b) VPIN-HS, and (c) VPIN-HE devices. The X-ray dose corresponding to each trace color is indicated in the legend inset in (a).

III. Results and Discussion

A. Geometric Dependence of TID Effects

Fig. 2 shows the *I*–*V* characteristics of representative VPIN-UHS, VPIN-HS, and VPIN-HE test structures after each 10-keV X-ray irradiation step with the sample grounded during irradiation. As seen from the reverse bias current regime, the dark current magnitude increases with TID for each device structure, especially in the range from 0 to −1 V. However, the dark current decrease at −2 V with increasing TID was observed in some of the devices. The effect observed is small and might be due to surface effects at higher reverse bias with the increase in oxide-trapped charge at the Ge/SiO_2 and/or Si/SiO_2 interfaces and a detailed study of these lies beyond the scope of this work. The standard operating voltage (−1 V) is used for all analysis of the degradation mechanisms of the photodiodes. Qualitatively, among the three photodiode structures, VPIN-HE exhibits the most pronounced dark current increase, suggesting a higher susceptibility to TID effects. This observation is supported in Fig. 3(a), which shows the dark current at −1 V, as a function of total dose for each VPIN design. VPIN-HE shows more than two times the increase in dark current compared to VPIN-UHS and VPIN-HS devices.

To evaluate the impact of geometry on TID response, the relative dark current increase with TID is computed using

$$\frac{\Delta I_{DC}}{I_0} = \frac{I_{\mathrm{rad}} - I_{\mathrm{pre-rad}}}{I_{\mathrm{pre-rad}}} \tag{1}$$

where I_{rad} is the dark current at each irradiation step and $I_{\mathrm{pre-rad}}$ is the dark current before irradiation. This normalization provides a comparative reference between the three VPIN designs, which have different sensitive volumes, as shown in Fig. 3(b). VPIN-UHS and VPIN-HS exhibit moderate increase in dark current of 6.9 nA (70%) and 6.7 nA (60%) at 2 Mrad(SiO_2), respectively, at −1 V. Since VPIN-UHS has the smallest sensitive volume of the three designs, while VPIN-HS has the largest, we rule out dependence of the radiation response on the sensitive volume. Conversely, the dark current increase for VPIN-HE, which has localized p^+ contact doping implants, is 13.6 nA (160%) at −1 V, indicating a more pronounced sensitivity to ionization-induced trapped charges at the Ge/SiO_2 interface.

While VPIN-HE exhibits lower dark current in practical operation up to 500 krad(SiO_2), the dark current increases relatively more compared to its pre-irradiation starting point compared to other geometries at operating voltage. The

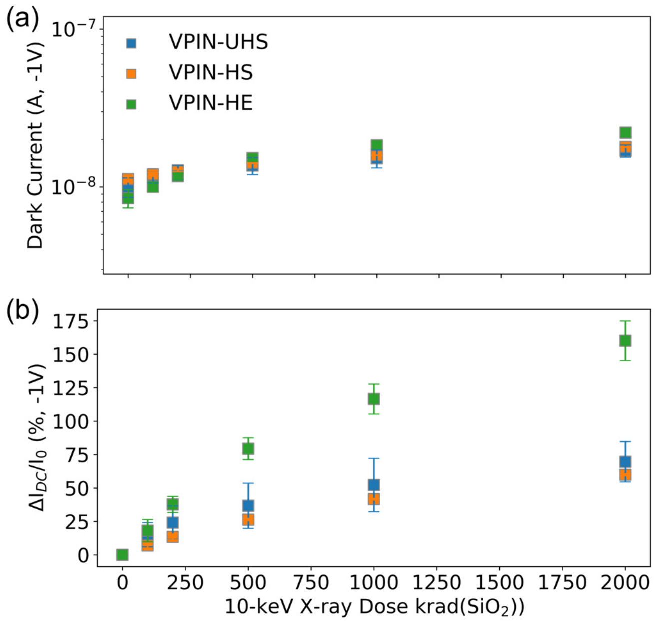

Fig. 3. Summary of 10-keV X-ray irradiation results with all devices grounded during exposure. (a) Dark current taken at −1 V and (b) relative increase in dark current ($\Delta I_{DC}/I_0$) at −1 V (expressed as percentage) as a function of TID. The mean (marker) and standard error (error bars) are indicated in blue (VPIN-UHS), orange (VPIN-HS), and green (VPIN-HE).

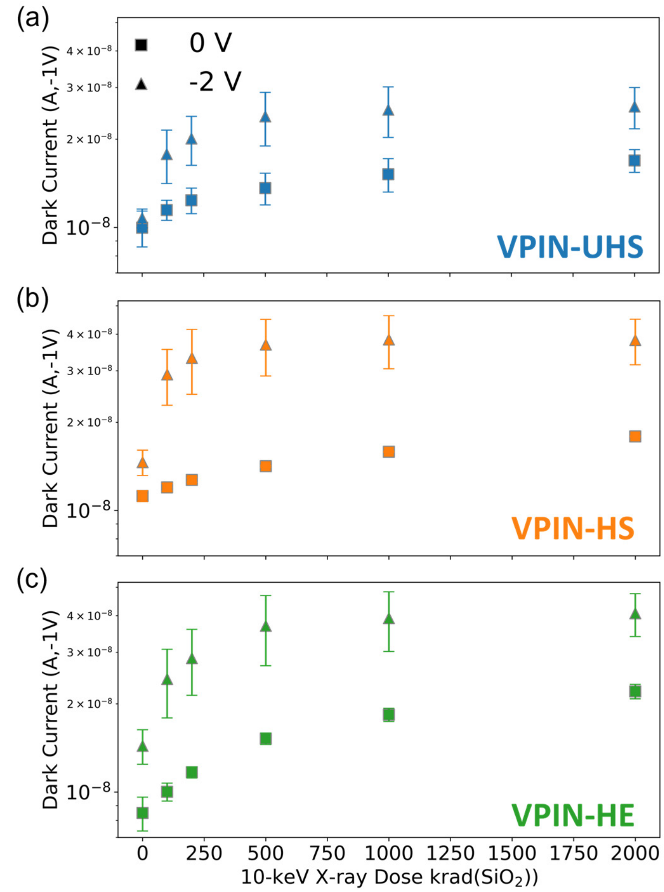

Fig. 4. Comparison of absolute increase in dark current (I_{DC}) at −1 V with respect to X-ray dose when the device is grounded (■) or biased at −2 V (▲) during irradiation for (a) VPIN-UHS, (b) VPIN-HS, and (c) VPIN-HE devices. The mean (marker) and the standard error (error bars) are plotted for each bias condition.

relative increase in dark current observed in VPIN-HE is approximately 90% (2.2 dB) higher than that observed in both VPIN-HS and VPIN-UHS. This significant increase is attributed to positive oxide-trapped charges located at the Ge/SiO_2 interface, particularly at the top corner region [32]. These trapped charges induce a pronounced local enhancement of the electric field, intensifying Shockley–Read–Hall (SRH) and trap-assisted tunneling (TAT) processes near the top p^+Ge/i-Ge junction, resulting in elevated dark currents [32].

VPIN-UHS and VPIN-HS exhibit comparable increases in dark current despite differing intrinsic Ge widths because irradiation-induced trapped charges predominantly affect SRH/TAT processes near the p^+Ge/i-Ge junction at the top Ge/SiO2 interface. Although VPIN-HS and VPIN-HE have similar Ge/SiO_2 interface area-to-perimeter ratios, the primary structural difference influencing TID sensitivity is the localized p^+ doping in VPIN-HE compared to continuous p^+ doping in VPIN-HS/UHS. The localized p^+ doping configuration in VPIN-HE increases the perimeter of the p^+-Ge/i-Ge junction near the Ge/SiO_2 interface that is susceptible to trapped charge-induced modifications, thereby enhancing its vulnerability to TID effects.

In contrast, the continuous p^+ doping in the VPIN-UHS and VPIN-HS devices mitigates the impact of positive oxide-trapped charges in that region by electrostatically screening the sensitive space-charge region [33]. Hence, the design choice of VPIN-HE to use localized p^+ doping to enhance photodiode efficiency inadvertently leads to increased sensitivity to TID. This underscores an inherent tradeoff observed in these VPIN devices under grounded irradiation between photodiode performance at operating voltage and radiation tolerance, necessitating careful consideration depending on specific application requirements.

B. Bias Dependence of TID Effects

Samples were also tested following X-ray irradiation at a bias of −2 V to investigate the effects of applied electric field on the TID response of Ge-Si VPIN PDs. We note that these Ge-Si VPIN PDs are designed to operate in the range 0 to −2 V; no voltage stress-induced degradation is observed in these devices over this bias range at room temperature [34]. Figs. 4 and 5 show the absolute and relative dark current increase at −1 V, respectively, as a function of total dose for each VPIN design with 0- and −2 V applied bias during irradiation. The error bars for the −2 V biased irradiation experiments are larger, which is attributed to higher pre-rad dark current and variability of the sample distribution. Of the three designs, VPIN-HE was the most sensitive under 0 V irradiation (as in Fig. 3) and experiences the greatest effect on dark current sensitivity during −2 V irradiation, with a relative dark current increase of 183% (−2 V) compared to 160% (grounded), showing increase in the sensitivity for active testing conditions. For VPIN-UHS and VPIN-HS, the relative dark current increase is 140% (−2 V) compared to 70%

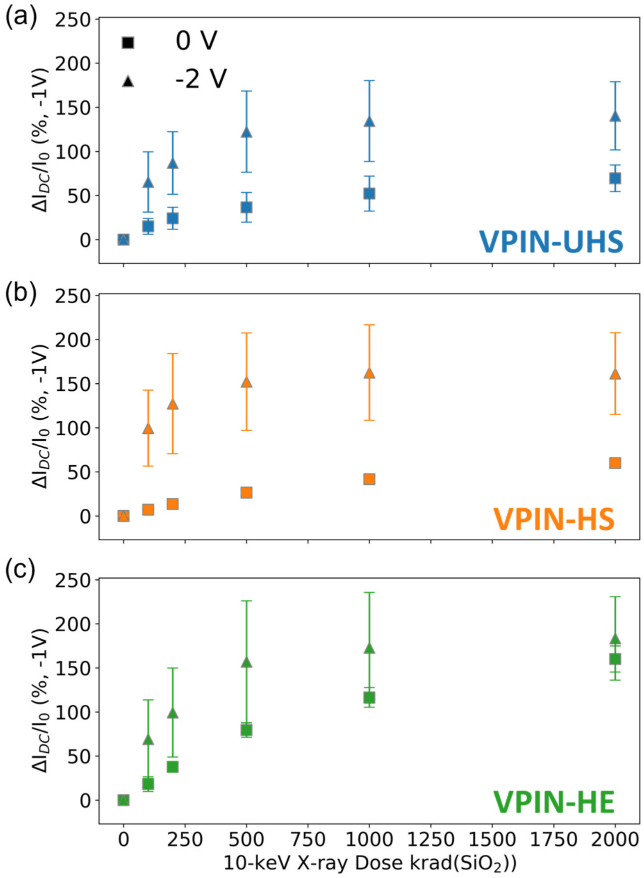

Fig. 5. Comparison of relative increases in dark current ($\Delta I_{DC}/I_0$) at −1 V expressed as a percentage with respect to X-ray dose when the device is grounded (■) or biased at −2 V (▲) during irradiation for (a) VPIN-UHS, (b) VPIN-HS, and (c) VPIN-HE devices. The mean (marker) and the standard error (error bars) are plotted for each bias condition.

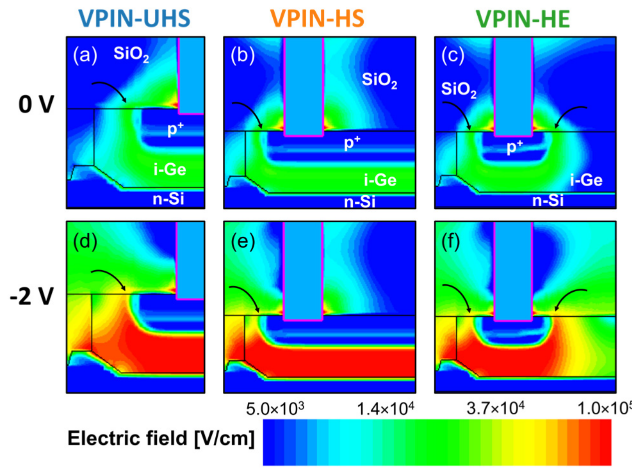

Fig. 6. Simulated pre-irradiation electric field profiles for biases of 0 and −2 V for (a) and (d) VPIN-UHS, (b) and (e) VPIN-HS, and (c) and (f) VPIN-HE devices, respectively. Black arrows indicate the electric field directions in SiO_2.

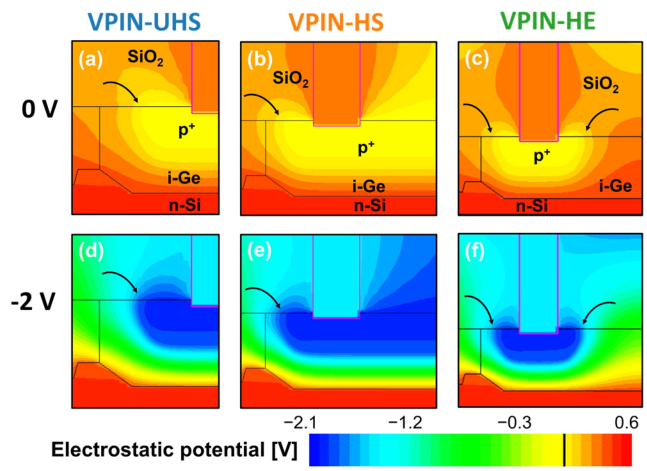

Fig. 7. Simulated pre-irradiation electrostatic potential profiles at biases of 0 and −2 V for the (a) and (d) VPIN-UHS, (b) and (e) VPIN-HS, and (c) and (f) VPIN-HE devices, respectively. Black arrows indicate the direction of the electrostatic potential gradient in SiO_2. The black line on the color bar indicates "zero" potential.

(grounded) and 161% (−2 V) compared to 60% (grounded), respectively.

The relative dark current increases observed during biased irradiation are similar across the three photodiodes, in contrast to the larger variation seen under grounded conditions, indicating a more consistent trapped charge distribution near the Ge/SiO2 interface. When biased at −2 V during irradiation, the observed dark current increase corresponds to an additional ~2 dB rise in the system noise floor compared to grounded irradiation. This emphasizes not only the importance of evaluating TID effects under realistic operating conditions, but also the potential cumulative impact on overall PIC performance, where even modest increases in device noise can become significant as circuit complexity increases.

Figs. 6 and 7 present the TCAD-simulated pre-irradiation electrostatic potential and electric field distributions at 0 and −2 V for the three Ge-Si VPIN PDs. At −2 V bias, a significant increase in electric field in the oxide and a stronger electrostatic potential gradient near the Ge/SiO_2 interface are observed compared to 0 V bias condition. This elevated electric field during irradiation enhances the trapping rate of charge close to the Ge/SiO_2 interface across all three devices [24], [35], [36], [37]. The resulting increase in trapped charge density contributes to higher TID sensitivity in the Ge-Si VPIN PDs. Consequently, the TID sensitivity under operating bias conditions is greater than that observed when the devices are grounded.

C. Annealing

As reported by Arnold et al. [26], the dark current degradation due to 10-keV X-ray irradiation of Ge-Si VPIN-HS photodiodes recovers within 24 h after irradiation. However, in our measurements, no recovery was observed after 24 h without forward bias. Since the measurement sequence in [26] includes a forward bias portion of the *I–V* sweep, which we believe facilitated the reported recovery, we subsequently explored forward bias-induced recovery. To investigate annealing kinetics in Ge-Si VPINs, samples were monitored after 2 Mrad(SiO_2) irradiation while grounded. Following the completion of irradiation, one device of each VPIN design was monitored for 15 min, measuring the dark current at −1 V every 5 s. As shown in Fig. 8, the dark current level was stable for each 15-min duration. After 15 min, an *I–V* sweep

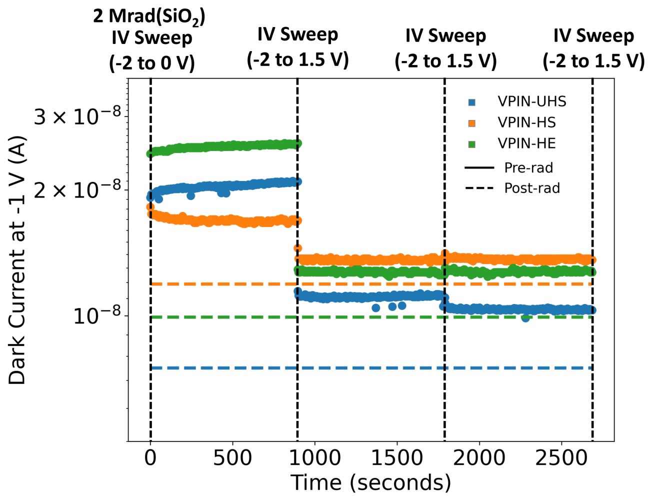

Fig. 8. Dark current at −1 V after a total dose of 2 Mrad(SiO_2) over time (I–V sweep from −2 to 1.5 V is performed after every 15 min). The type of device structure is indicated in the legend. One representative sample of each device configuration is shown.

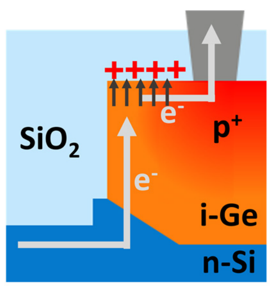

Fig. 9. Schematic cross section of Ge-Si VPIN photodiode under forward bias, illustrating the movement of electrons toward the contact. The forward bias neutralizes ionization-induced trapped charges at the top-corner Ge/SiO_2 interface due to tunneling electrons.

was performed from −2 to 1.5 V; the dark current partially recovers within one sweep. This monitoring procedure was repeated three times, with a full I–V sweep performed before resuming dark current monitoring at −1 V. The time required to perform a full I–V sweep was less than 5 s. The dark current partially recovers within one full I–V sweep from −2 to 1.5 V but does not recover further for each subsequent sweep interval. This suggests that most shallow trapped charges at the Ge/SiO_2 interface are neutralized by room temperature electron tunneling during the forward bias portion of the first I–V sweep itself [35], [36].

Forward current-induced recovery of Ge-Si photodiodes has been reported in previous studies [28], suggesting forward injection may be utilized to mitigate radiation-induced degradation. Dark current recovery due to forward injection was observed in both test cases where devices were biased and grounded during irradiation, suggesting that most of the trapped charge forms near the Ge/SiO_2 interface irrespective of bias applied during irradiation and contributes dominantly to the noise floor susceptibility of each device. In fact, post recovery relative dark current increase is less than 50% in both cases with the application of forward bias I–V sweeps after irradiation.

Fig. 9 illustrates this movement of electrons during forward bias, flowing near the top corner Ge/SiO_2 interface, which results in the neutralization of ionization-induced trapped charges. The results highlight that partial noise floor recovery can be effectively achieved for practical implementations of PICs in space systems by applying a short duration forward bias voltage exceeding the diode threshold.

IV. Summary and Conclusion

The impacts of device geometry and bias on TID effects in three different types of VPIN Ge-Si photodiodes optimized for different speed and efficiency metrics were evaluated during 10-keV X-ray irradiation. Under grounded irradiation, photodiodes exhibiting localized p^+ contact doping (VPIN-HE) showed the highest susceptibility to TID at −1 V, with a relative dark current increase greater than twice that of photodiodes with continuous p^+ contact implants, which was attributed to a larger sensitive area near the top Ge/SiO_2 interface. While VPIN-HE shows the best absolute dark current performance up to 500 krad(SiO_2), the dark current increase is more relative to its pre-irradiation starting point compared to other geometries. However, under biased irradiation, all the photodiodes show similar relative increase in dark current at −1 V. All devices exhibit ~2 dB increase in noise floor compared to grounded irradiation due to increased electric field near the Ge/SiO_2 interfaces. Forward-injection-induced dark current recovery was observed during I–V sweeps (−2 to 1.5 V), which facilitated the neutralization of shallow-trapped charge via room temperature electron tunneling. Slightly more than 60% recovery was shown for all devices. These considerations must be weighed alongside pre-existing performance tradeoffs when selecting an appropriate photodiode for PIC design in aerospace applications. This study highlights the importance of evaluating radiation sensitivity under conditions that simulate the practical operation of devices and systems in space and high-energy physics PIC applications, as well as the impact of design on radiation sensitivity.

Acknowledgment

Andrew Sternberg, James Trippe, Phoenix Harris, Michael McCurdy, Colin Bryant, Nathaniel Karom, and Jacopo Franco are thanked for their support in the experimental setup and for technical discussions. John Fellenstein of the Vanderbilt Physics Machine Shop is acknowledged for assistance in the fabrication of components crucial to the success of the experiments performed in this study. The imec 200 mm pilot-line and the imec industrial affiliation Research and Development Program on Optical I/O are acknowledged for platform fabrication and technical support.

References

[1] Y. Shi et al., "Silicon photonics for high-capacity data communications," *Photon. Res.*, vol. 10, no. 9, pp. A106–A134, Sep. 2022.

[2] S. Shekhar et al., "Roadmapping the next generation of silicon photonics," *Nat. Commun.*, vol. 15, no. 1, Jan. 2024, Art. no. 751.

[3] V. Stojanović et al., "Monolithic silicon-photonic platforms in state-of-the-art CMOS SOI processes," *Opt. Exp.*, vol. 26, no. 10, pp. 13106–13121, May 2018.

[4] R. Mahajan et al., "Co-packaged photonics for high performance computing: Status, challenges and opportunities," *J. Lightw. Technol.*, vol. 40, no. 2, pp. 379–392, Jan. 15, 2022.

[5] S. Lischke et al., "High bandwidth, high responsivity waveguide-coupled germanium p-i-n photodiode," *Opt. Exp.*, vol. 23, no. 21, pp. 27213–27220, Oct. 2015.

[6] H. T. Chen et al., "High-responsivity low-voltage 28-Gb/s Ge p-i-n photodetector with silicon contacts," *J. Lightw. Technol.*, vol. 33, no. 4, pp. 820–824, Feb. 15, 2015.

[7] M. A. Krainak et al., "Integrated photonics for NASA applications," *Proc. SPIE*, vol. 10899, pp. 75–94, Mar. 2019.

[8] G. N. Tzintzarov, S. G. Rao, and J. D. Cressler, "Integrated silicon photonics for enabling next-generation space systems," *Photonics*, vol. 8, no. 4, p. 131, Apr. 2021.

[9] G. Terrasanta, M. W. Ziarko, N. Bergamasco, M. Poot, and J. Poliak, "Photonic integrated circuits for optical satellite links: A review of the technology status and space effects," *Int. J. Satell. Commun. Netw.*, vol. 43, no. 3, pp. 210–228, Jun. 2025.

[10] Q. Du, "High energy radiation damage on silicon photonic devices: A review," *Opt. Mater. Exp.*, vol. 13, no. 2, pp. 403–412, Feb. 2023.

[11] C. Barnes, G. Swift, A. Johnston, B. Rax, and K. LaBel, "Radiation effects considerations for the application of photonics in space systems," in *Proc. IEEE Aerosp. Conf.*, Snowmass, CO, USA, Mar. 1998, pp. 219–239.

[12] G. N. Tzintzarov et al., "Direct measurement of total-ionizing-dose-induced phase shifts in commercially available, integrated silicon-photonic waveguides," *IEEE Trans. Nucl. Sci.*, vol. 70, no. 8, pp. 2116–2124, Aug. 2023.

[13] S. Grillanda et al., "Gamma radiation effects on silicon photonic waveguides," *Opt. Lett.*, vol. 41, no. 13, pp. 3053–3056, Jul. 2016.

[14] N. Boynton et al., "Gamma radiation effects on passive silicon photonic waveguides using phase sensitive methods," *Opt. Exp.*, vol. 28, no. 23, pp. 35192–35201, Nov. 2020.

[15] I. Reghioua et al., "Radiation effects on Si-photonics-integrated passive devices: Postirradiation measurements," *IEEE Trans. Nucl. Sci.*, vol. 70, no. 8, pp. 1973–1981, Aug. 2023.

[16] M. Lalovic et al., "Ionizing radiation effects in silicon photonics modulators," *IEEE Trans. Nucl. Sci.*, vol. 69, no. 7, pp. 1521–1526, Jul. 2022.

[17] M. Zeiler et al., "Radiation damage in silicon photonic Mach–Zehnder modulators and photodiodes," *IEEE Trans. Nucl. Sci.*, vol. 64, no. 11, pp. 2794–2801, Nov. 2017.

[18] M. Hosseinzadeh et al., "Analysis of optical single-event transients in integrated silicon photonics Mach–Zehnder modulators for space-based optical communications," *IEEE Trans. Nucl. Sci.*, vol. 71, no. 4, pp. 736–743, Apr. 2024.

[19] A. Kraxner et al., "Investigation of the influence of temperature and annealing on the radiation hardness of silicon Mach–Zehnder modulators," *IEEE Trans. Nucl. Sci.*, vol. 65, no. 8, pp. 1624–1631, Aug. 2018.

[20] M. Hosseinzadeh et al., "Total-ionizing-dose effects in integrated silicon phase shifters using localized X-ray pulses," *IEEE Trans. Nucl. Sci.*, vol. 72, no. 4, pp. 1172–1180, Apr. 2025.

[21] S. Bhandaru, S. Hu, D. M. Fleetwood, and S. M. Weiss, "Total ionizing dose effects on silicon ring resonators," *IEEE Trans. Nucl. Sci.*, vol. 62, no. 1, pp. 323–328, Feb. 2015.

[22] G. Terrasanta, A. M. Zinth, M. W. Ziarko, N. Bergamasco, J. Poliak, and M. Poot, "Total ionizing dose effects on silicon nitride photonic integrated microring resonators and Mach–Zehnder interferometers," *IEEE Trans. Nucl. Sci.*, vol. 72, no. 4, pp. 1542–1551, Apr. 2025.

[23] L. D. Ryder, R. D. Schrimpf, R. A. Reed, and S. M. Weiss, "Radiation-induced transient response mechanisms in photonic waveguides," *IEEE Trans. Nucl. Sci.*, vol. 69, no. 3, pp. 546–557, Mar. 2022.

[24] G. N. Tzintzarov et al., "Single-event transients in a commercially available, integrated germanium photodiode for silicon photonic systems," *IEEE Trans. Nucl. Sci.*, vol. 69, no. 3, pp. 527–533, Mar. 2022.

[25] P. S. Goley et al., "Total ionizing dose effects in 70-GHz bandwidth photodiodes in a SiGe integrated photonics platform," *IEEE Trans. Nucl. Sci.*, vol. 66, no. 1, pp. 125–133, Jan. 2019.

[26] K. P. Arnold et al., "Displacement damage and ionization effects on waveguide-integrated germanium-silicon p-i-n photodiodes," *IEEE Trans. Nucl. Sci.*, vol. 72, no. 4, pp. 1181–1190, Apr. 2025.

[27] P. S. Goley, N. A. Dodds, M. Frounchi, G. N. Tzintzarov, R. N. Nowlin, and J. D. Cressler, "Response of waveguide-integrated germanium-on-silicon p-i-n photodiodes to neutron displacement damage," *IEEE Trans. Nucl. Sci.*, vol. 67, no. 1, pp. 296–304, Jan. 2020.

[28] L. Olanterä et al., "Effects of high fluence particle irradiation on germanium-on-silicon photodiodes," *IEEE Trans. Nucl. Sci.*, vol. 71, no. 4, pp. 728–735, Apr. 2024.

[29] F. Ferraro et al., "Imec silicon photonics platforms: Performance overview and roadmap," *Proc. SPIE*, vol. 12429, pp. 22–28, Mar. 2023, Art. no. 1242909.

[30] S.-H. Chen et al., "ESD robustness of germanium photodetectors in advanced silicon photonics technology," in *Proc. 46th Annu. EOS/ESD Symp. (EOS/ESD)*, Sep. 2024, pp. 1–7.

[31] M. Pantouvaki et al., "Active components for 50 Gb/s NRZ-OOK optical interconnects in a silicon photonics platform," *J. Lightw. Technol.*, vol. 35, no. 4, pp. 631–638, Feb. 15, 2017.

[32] S. Musibau et al., "Fundamental mechanisms of total-ionizing-dose degradation in waveguide-coupled germanium-on-silicon p-i-n photodetectors," *IEEE Trans. Nucl. Sci.*, early access, doi: 10.1109/TNS.2025.3628718.

[33] H. J. Barnaby, "Total-ionizing-dose effects in modern CMOS technologies," *IEEE Trans. Nucl. Sci.*, vol. 53, no. 6, pp. 3103–3121, Dec. 2006.

[34] S. Musibau et al., "Degradation and recovery kinetics study of vertical and lateral Ge-on-Si photodetectors," in *Proc. IEEE Int. Rel. Phys. Symp. (IRPS)*, Apr. 2024, pp. 41–50.

[35] T. R. Oldham and F. B. McLean, "Total ionizing dose effects in MOS oxides and devices," *IEEE Trans. Nucl. Sci.*, vol. 50, no. 3, pp. 483–499, Jun. 2003.

[36] D. M. Fleetwood, "Total ionizing dose effects in MOS and low-dose-rate-sensitive linear-bipolar devices," *IEEE Trans. Nucl. Sci.*, vol. 60, no. 3, pp. 1706–1730, Jun. 2013.

[37] C. X. Zhang et al., "Effect of ionizing radiation on defects and *1/f* noise in Ge pMOSFETs," *IEEE Trans. Nucl. Sci.*, vol. 58, no. 3, pp. 764–769, Jun. 2011.